Journal of Zhejiang University-SCIENCE A (Applied Physics & Engineering)
ISSN 1673-565X (Print); ISSN 1862-1775 (Online)
www.zju.edu.cn/jzus; www.springerlink.com
E-mail: jzus@zju.edu.cn

Theoretical elastoplastic analysis for foundations with geosynthetic-encased columns*

Yuan-yu DUAN[1], Yi-ping ZHANG†‡1, Dave CHAN[2], Ya-nan YU[1]

([1]*College of Civil Engineering and Architecture, Zhejiang University, Hangzhou 310058, China*)

([2]*Department of Civil and Environmental Engineering, University of Alberta, Edmonton, Alberta, Canada*)

†E-mail: zhangyiping@zju.edu.cn

Received Dec. 19, 2011; Revision accepted May 15, 2012; Crosschecked May 29, 2012

Abstract: As a new technique in ground improvement, geosynthetic-encased columns (GECs) have promising applications in soft soil foundation. By assuming yielding occurs in the columns while the surrounding soil and the geosynthetic remain elastic, an elastoplastic analytical procedure for foundations improved by GECs is proposed. The radial stresses that the geosynthetic provides and the elastoplastic deformations of the foundation resting on a rigid base are derived. A comparison with finite element analysis shows that the proposed method is effective and can provide a reasonable prediction of a GEC's deformation. Subsequent parametric analysis indicates that higher geosynthetic stiffness leads to better performance of the composite foundation. The optimum length of encasement is related to the load acting on the foundation and the permissible vertical and radial displacements of the column. Moreover, as the dilation angle of the column increases, the settlement decreases, especially under high loading. The influence of the encasement is more significant in soils with smaller elastic modulus.

Key words: Geosynthetic-encased columns (GECs), Equal vertical strain, Elastoplastic deformation, Analytical procedure
doi:10.1631/jzus.A1100334 **Document code:** A **CLC number:** TU4

1 Introduction

Granular columns are widely used for supporting flexible structures such as embankments and storage tanks which are sited on soft ground. Granular columns can improve the bearing capacity, reduce foundation settlement, and increase the time rate of settlement. Granular columns have been proven successful in soft soils with undrained shear strength of >15 kPa. However, bulging failure of the columns can occur due to a lack of lateral confinement. To extend the applicability of granular columns to very soft soils, van Impe and Silence (1986) suggested the use of a geosynthetic to encase the columns. A geosynthetic provides the desired lateral support for the granular materials, therefore improving the performance of the columns.

There have been many studies of the performance of geosynthetic-encased columns (GECs). Due to the difficulty of deriving analytical solutions for GECs, however, most studies have been conducted using a model test or numerical simulation. Model tests are effective for investigating the performance of a single GEC or a GEC's composite foundation. Rajagopal *et al.* (1999) performed a large number of triaxial compression tests on granular columns encased in single and multiple geocells. Their study was focused on the strength of the encased-column, but they did not consider the load-deform relationship of the encased-column or the interaction between the column and the surrounding soil. Kempfert *et al.* (1999) conducted experimental investigations of the bearing capacity and deformation of GECs using large- and small-scale model tests under static and cyclic loading. Ayadat and Hanna (2005) reported the

‡ Corresponding author
* Project (No. 2011FZA4021) supported by the Fundamental Research Funds for the Central Universities, China

load carrying capacity and settlement characteristics of GECs installed in a collapsible soil layer, based on experimental investigations. To investigate the qualitative and quantitative improvement of the load capacity of individual encased stone columns, Murugesan and Rajagopal (2007; 2010) performed laboratory model tests on a rigid unit cell and laboratory model tests on a group of stone columns with or without encasement. All these studies used geotextiles as the encasement material. However, other geosynthetic materials, such as geogrid, can also be used. A series of small-scale model column tests were conducted by Gniel and Bouazza (2009) to investigate the behavior of geogrid encased columns. Their experiments were focused on the effect of varying the length of the encasement and on the difference in behavior between a single encased column and a group of columns. Gniel and Bouazza (2010) then proposed a method of geogrid encasement construction and conducted a series of small-scale and medium-scale compression tests to investigate their technique.

Numerical analysis is also commonly used to investigate the performance of GECs. Murugesan and Rajagopal (2006) investigated the qualitative and quantitative improvement in load capacity of a stone column by encasement, using a comprehensive parametric study involving finite element analysis. Malarvizhi and Ilamparuthi (2008) simulated triaxial tests on encapsulated stone columns and evaluated the behavior of a composite system using finite element analysis and PLAXIS software. The findings from a series of numerical studies on the contribution of geosynthetic encasement to the enhancement of the performance of stone columns in very soft clay soil were compiled by Lo *et al*. (2010). 3D finite element analyses were carried out to simulate the behavior of a single GEC in very soft clay using the software ABAQUS, and the influence of various factors on the performance of GECs were discussed by Khabbazian *et al.* (2009; 2010a; 2010b). Compared to model tests, numerical analysis can consider more complicated boundary conditions and investigate the influence of different factors. However, neither model tests nor numerical simulation can provide a convenient design method for GEC foundations, so the theoretical method appears very important.

Compared with experimental and numerical studies on GECs, theoretical analysis is lagging behind. Assuming that a composite foundation with GECs satisfies the equal strain condition and rests on a rigid layer, and that the volume of the column remains constant, an analytical solution for deformations of GECs has been developed by Raithel and Kempfert (2000). Wu *et al.* (2009) adopted the Duncan and Chang model to describe the mechanical characteristics of the granular materials and establish the analytical procedures to investigate the axial stress-strain response of GECs. Their proposed analytical method was verified by subsequent triaxial compression tests (Wu and Hong, 2009). Based on the unit cell model and displacement governing equations, Zhang *et al.* (2011) proposed a theoretical elastic solution of stresses and displacements of a composite foundation with GECs. However, these analytical studies were based on elasticity theory, which is unrealistic. Recently, as an extension of Balaam and Booker (1985)'s classical elastoplastic analytical procedures for foundations with granular columns, Pulko *et al.* (2011) developed an analytical closed-form elastoplastic solution for a fully encased column. However, the effect of the radial stresses at different locations on the radial deflection of the soil was ignored to simplify calculation, and this simplification made their method inappropriate in the case of a partially encased granular column.

To develop a more reasonable calculation method for a GEC composite foundation, by assuming yielding occurs in columns while the surrounding soil and the geosynthetic remain elastic, this paper presents a more applicable analytical procedure for not only fully encased granular columns but also partially encased granular columns. To validate the derived solution, finite element analysis was carried out using PLAXIS, and the results show very good agreement with the analytical solution. Subsequently, parametric analyses based on the elastoplastic solution were carried out to study the effect of various factors on the performance of composite foundations with GECs.

2 Methods of analysis system design

2.1 Mathematical model

The unit cell model in this study is composed of a granular column, a geosynthetic and surrounding

soil (Fig. 1). The computational model has a radius r_c of the column, a radius r_e of the surrounding soil, a height h of the unit cell, and a length h_f of the geosynthetic. A uniform load of p_0 acts on the smooth rigid raft over the unit cell.

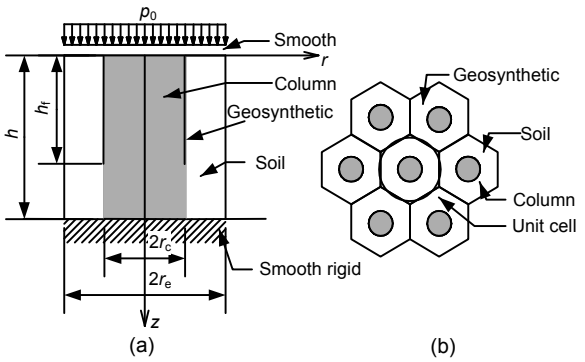

Fig. 1 Unit cell model
(a) Profile map; (b) Plane-view

The following assumptions are made:

1. The column-geosynthetic-soil system is sited on a smooth and rigid base.

2. The equal strain hypothesis is satisfied, i.e., the horizontal sections of the unit cell model remain horizontal in the course of settlement. Previous studies (Balaam and booker, 1985; Raithel and Kempfert, 2000; Wu and Hong, 2009; Pulko *et al.*, 2011; Zhang *et al.*, 2011) also made this assumption. Although the equal strain hypothesis is not applicable in all cases, it is most appropriate in cases when the end bearing is rigid or the column space is small. By making this assumption, we can infer that there is no shear stress at the column-geosynthetic-soil interfaces.

3. The column material is an elastic-perfectly plastic solid satisfying the Mohr-Coulomb yield criterion while the surrounding soil and the geosynthetic are assumed to be linear-elastic and homogeneous.

4. Compressive stresses and deformations are taken as positive.

The model for elastoplastic analysis of the unit cell is shown in Fig. 2. The displacements and stresses of the column, the geosynthetic, and the surrounding soil are analyzed separately.

2.2 Analysis of the soil

The surrounding soil, geosynthetic and column are all subdivided into a number of cylinders, $z_i \le z \le z_{i+1}$, $i=1, 2, \cdots, n$, and the radial stress on the inner surface of each soil element and on the outer surface of each column element are assumed to be constants and equal to $(\sigma_{rs})_i$ and $(\sigma_{rc})_i$, respectively (Fig. 2).

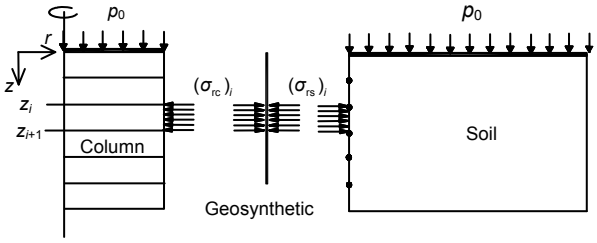

Fig. 2 Model of elastoplastic analysis

Since the soil remains elastic, based on the superposition principle of elastic theory, the average radial deflection ρ_i of the ith element ($z_i \le z \le z_{i+1}$) is the sum of the average radial deflection $(\rho_1)_i$ caused by radial stress and the average radial deflection $(\rho_2)_i$ caused by vertical displacement δ (Fig. 3), and is given by Balaam and Booker (1985) as

$$\rho_i = (\rho_1)_i + (\rho_2)_i = \sum_{j=1}^{n} A_{ij} R_j + \theta\delta, \tag{1}$$

where $R_j = 2\pi\Delta z_j r_c (\sigma_{rs})_j$ is the total force on the inner surface of the jth element ($z_j \le z \le z_{j+1}$), and the coefficient A_{ij} is as shown in the Appendix. According to the elastic solution (Zhang *et al.*, 2011), the coefficient θ is given by

$$\theta = \frac{r_c B}{h}\left(1 - \frac{r_e^2}{r_c^2}\right), \tag{2}$$

where $B = \lambda_s \Big/ \left\{2\left[\lambda_s + G_s\left(1 + r_e^2/r_c^2\right)\right]\right\}$, where λ_s and G_s are Lame's parameters of the soil. Similarly, the force carried by the surrounding soil can be expressed as (Balaam and Booker, 1985)

$$F_s = (F_s)_1 + (F_s)_2 = \sum_{j=1}^{n} \theta' R_j - \xi\delta. \tag{3}$$

It is found that $\theta' = -\theta$ due to reciprocal theorem and Eq. (3) is rewritten as

$$F_s = -\sum_{j=1}^{n} \theta R_j - \xi\delta, \tag{4}$$

where the coefficient ξ is given by

$$\xi=\frac{\pi(r_e^2-r_c^2)}{h}\left[2\lambda_s B-(\lambda_s+2G_s)\right]. \tag{5}$$

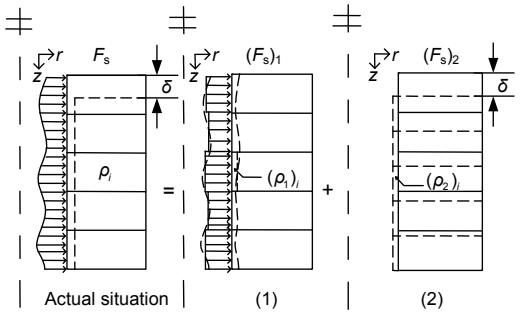

Fig. 3 Schematic diagram of analysis of the soil

2.3 Analysis of the encasement

A geosynthetic of length h_f can be subdivided into n_f elements. Based on the condition of static equilibrium (Fig. 4), the average radial stress that the geosynthetic imposes on the column over the ith element ($z_i \le z \le z_{i+1}$, $i=1, 2, \cdots, n_f$) is given by

$$\sigma_{fi}=(\sigma_{rc})_i-(\sigma_{rs})_i=J_f\frac{\rho_i}{r_c(r_c+\rho_i)}, \tag{6}$$

where J_f is the stiffness of the encasement. Since ρ_i is far less than r_c, then $r_c(r_c+\rho_i)\approx r_c^2$, and Eq. (6) can be simplified as

$$\sigma_{fi}=\frac{J_f\rho_i}{r_c^2}. \tag{7}$$

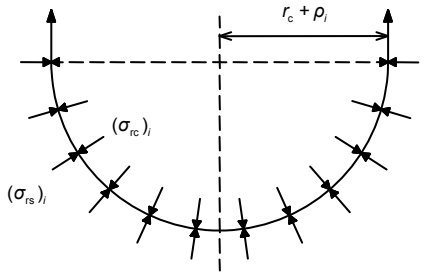

Fig. 4 Diagram showing the calculation of the radial stress of the encasement

2.4 Analysis of the column

According to the equal strain hypothesis, the shear stresses on the surfaces of the granular columns are negligible and the column is under triaxial stress condition ($\sigma_{rc}=\sigma_{\theta c}$). Similar to the analysis of the soil, the column is subdivided into n elements and the stresses of the jth element of the column ($z_j \le z \le z_{j+1}$) are given by

$$(\sigma_{zc})_j=\frac{F_c}{\pi r_c^2}, \tag{8}$$

$$\begin{aligned}(\sigma_{rc})_j&=(\sigma_{\theta c})_j=(\sigma_{rs})_j+\eta_j(\sigma_{rf})_j\\&=\frac{R_j}{2\pi r_c\Delta z_j}+\eta_j J_f\frac{\rho_j}{r_c^2},\end{aligned} \tag{9}$$

where F_c is the force carried by the column, and

$$\eta_j=\begin{cases}1, & j=1,2,\cdots,n_f,\\ 0, & j=n_f+1,n_f+2,\cdots,n.\end{cases}$$

The incremental strains of the column can be approximated by

$$\mathrm{d}\varepsilon_{rc}=\mathrm{d}\varepsilon_{\theta c}=-\frac{\mathrm{d}\rho_j}{r_c}. \tag{10}$$

The stress-strain increment relation is given in matrix form:

$$\begin{bmatrix}\mathrm{d}(\sigma_{zc})_j\\ \mathrm{d}(\sigma_{rc})_j\end{bmatrix}=G_c\begin{bmatrix}X_j & Y_j\\ Z_j & T_j\end{bmatrix}\begin{bmatrix}\mathrm{d}(\varepsilon_{zc})_j\\ 2\mathrm{d}(\varepsilon_{rc})_j\end{bmatrix}, \tag{11}$$

where G_c, E_c, and v_c are shear modulus, Young's elastic modulus, and Poisson's ratio of the column, respectively. When the element of the column is in an elastic state, the stress-strain relation complies with Hooke's law. Moreover, when the column material yields, the incremental stress-strain relationship satisfies the Mohr-Coulomb yield criterion with the non-associated flow rule.

The yield function can be expressed as

$$f=\sigma_1+c_c\cot\varphi_c-\frac{1+\sin\varphi_c}{1-\sin\varphi_c}(\sigma_3+c_c\cot\varphi_c), \tag{12}$$

where c_c is the cohesion strength, φ_c the angle of internal friction of the column material, and σ_1 and σ_3 the major and minor principal stresses, respectively.

The potential function used for the non-associated flow rule is:

$$g=\sigma_1-\frac{1+\sin\psi_c}{1-\sin\psi_c}\sigma_3, \tag{13}$$

where ψ_c is the angle of dilatancy of the column material.

The elastic elements and plastic elements of the matrix in Eq. (11) are shown in Table 1.

Table 1 Elastic and plastic elements of the stiffness matrix

Elastic element	Plastic element*
$X_j^e=\frac{2(1-\nu_c)}{1-2\nu_c}$	$X_j^{ep}=HMN$
$Y_j^e=\frac{2\nu_c}{1-2\nu_c}$	$Y_j^{ep}=HM$
$Z_j^e=\frac{2\nu_c}{1-2\nu_c}$	$Z_j^{ep}=HN$
$T_j^e=\frac{1}{1-2\nu_c}$	$T_j^{ep}=H$

* $H=\frac{2(1+\nu_c)}{2+MN-2\nu_c(1+M+N)}$, $M=\frac{1+\sin\varphi_c}{1-\sin\varphi_c}$, $N=\frac{1+\sin\psi_c}{1-\sin\psi_c}$

2.5 Governing equations

Substituting Eqs. (8)–(10) into Eq. (11), we can obtain:

$$\Delta z_j\left(\mathrm{d}\varepsilon_{zc}\right)_j=b_j\mathrm{d}F_c+f_j\mathrm{d}\rho_j, \tag{14}$$

$$\mathrm{d}R_j=c_j\mathrm{d}F_c-g_j\mathrm{d}\rho_j, \tag{15}$$

where $b_j=\Delta z_j/(\pi r_c^2X_jG_c)$, $f_j=2Y_j\Delta z_j/(X_jr_c)$, $c_j=2Z_j\Delta z_j/(X_jr_c)$, and $g_j=4\pi\Delta z_jG_c\left[\frac{(X_jT_j-Z_jY_j)}{X_j}+\frac{\eta_jJ_f}{2G_cr_c}\right]$.

If Eq. (15) is substituted into the incremental form of Eq. (1), it is found that

$$\sum_{j=1}^{n}\left(1+A_{ij}g_j\right)\mathrm{d}\rho_j-\left(\sum_{j=1}^{n}A_{ij}c_j\right)\mathrm{d}F_c-\theta_i\mathrm{d}\delta=0. \tag{16}$$

Eq. (14) can be used to calculate the settlement $\mathrm{d}\delta$ of the column:

$$\sum_{j=1}^{n}f_j\mathrm{d}\rho_j+\left(\sum_{j=1}^{n}b_j\right)\mathrm{d}F_c-\mathrm{d}\delta=0. \tag{17}$$

The increment of load acting on the unit cell $\mathrm{d}F=\mathrm{d}F_c+\mathrm{d}F_s$. According to Eqs. (4) and (15), we can obtain:

$$\sum_{j=1}^{n}\theta g_j\mathrm{d}\rho_j+\left(1-\sum_{j=1}^{n}\theta c_j\right)\mathrm{d}F_c-\xi\mathrm{d}\delta=\mathrm{d}F. \tag{18}$$

Eqs. (16)–(18) are composed of a set of n+2 equations with n+2 unknowns: $\mathrm{d}\rho_j$, $\mathrm{d}F_c$, and $\mathrm{d}\delta$. The equations can be solved when the applied load $\mathrm{d}F$ is given. Initially, both the column and the soil are in elastic equilibrium. As the load increases step by step, according to incremental plastic theory, the column elements become elastoplastic one by one. In each step, an appropriate load increment $\mathrm{d}F$ should be chosen so that only one additional element yields and the element is exactly on the verge of yielding at the end of the increment. In that case, the coefficients X_j, Y_j, Z_j, and T_j are independent of stress level, and an iteration is not needed (Balaam and Booker, 1985). The process of elastoplastic analysis is shown in Fig. 5.

3 Validation of the analysis model

To validate this approach, the results of the elastoplastic analysis were compared with the results of a finite element analysis of an axi-symmetric unit cell model of composite foundation using the software package PLAXIS. A rigid plate with a uniform load is applied to the top of the unit cell model to ensure uniform vertical displacements (Fig. 6a). Vertical constraint on the bottom boundary and horizontal constraint on the lateral boundaries are set. Geosynthetics are modeled by membrane elements which sustain only tensile forces and no compression. In order not to limit the final state of the soil and the column, both the column and the soil are set to be elastoplastic materials satisfying the Mohr-Coulomb yield criterion. Fifteen-noded triangular elements were used in the FEM analyses. The finite element

mesh is shown in Fig. 6b. The model parameters in the elastoplastic analysis and the FEM are shown in Table 2.

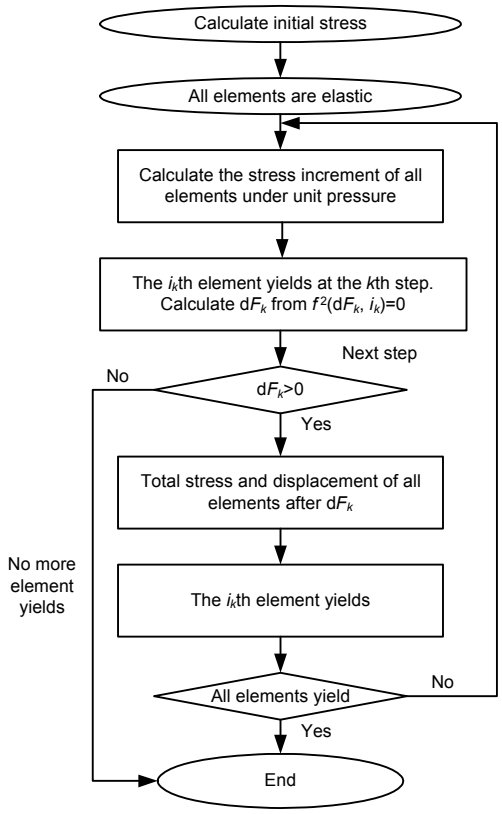

Fig. 5 Flow diagram of elastoplastic analysis

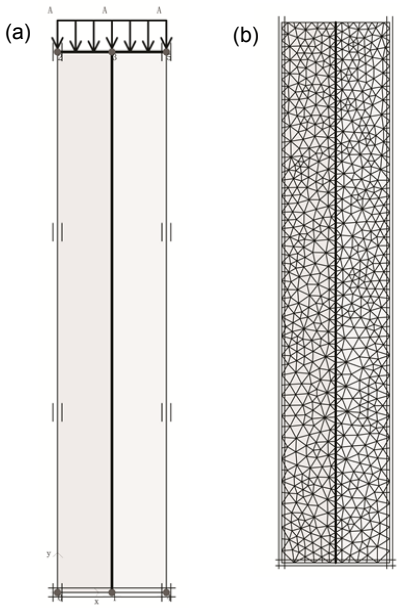

Fig. 6 Axi-symmetric unit cell model in PLAXIS
(a) Unit cell model; (b) Finite element mesh

Table 2 Parameters of models

Parameter	Value	
	Analytical method	FEM
r_c (m)	0.5	0.5
r_e (m)	1	1
h (m)	5	5
E_c (MPa)	60.0	60.0
E_s (MPa)	2.0	2.0
v_c	0.3	0.3
v_s	0.3	0.3
φ_c (°)	35	35
φ_s (°)	–	25
c_c (kPa)	0	0.01
c_s (kPa)	–	13.00
ψ_c (°)	5	5
ψ_s (°)	–	0

The load-settlement curves of the foundations with GECs and with ordinary granular columns (OGCs, i.e., without encasement) obtained by elastoplastic analysis, elastic analysis (Zhang *et al.*, 2011), and PLAXIS are shown in Fig. 7a. The radial displacements of the columns obtained by elastoplastic analysis and PLAXIS are shown in Fig. 7b. The results of the elastoplastic analysis agree well with those of the numerical analysis (Figs. 7a and 7b). This implies that the soil behaves as if it is in an elastic state during loading. Otherwise, the results of the FEM should deviate from those of the analytical methods, since it has been set as elastoplastic material in the numerical analyses. It also shows that the displacements of the composite foundation have been underestimated in the elastic analysis. This indicates that the influence of yielding in the column material cannot be neglected. The results demonstrate that the assumption that yielding occurs in columns while little yielding occurs in the soil is reasonable, and the presented elastoplastic analysis is feasible.

4 Parametric studies

To investigate the influence of the model parameters on the behavior of the composite foundation, parametric analyses were performed. The basic parameters of the model are listed in Table 2.

Note that δ_{elas} is the solution of the settlement of elastic analysis predicted by Zhang *et al.* (2011) and δ

is the solution of the settlement of elastoplastic analysis in this study. A plastic settlement correction factor N is defined as

$$N=\frac{\delta}{\delta_{\text{elas}}}. \tag{19}$$

The value of N reflects the effect of yielding of the column on the displacement. The bigger is the N value, the more significant is the effect.

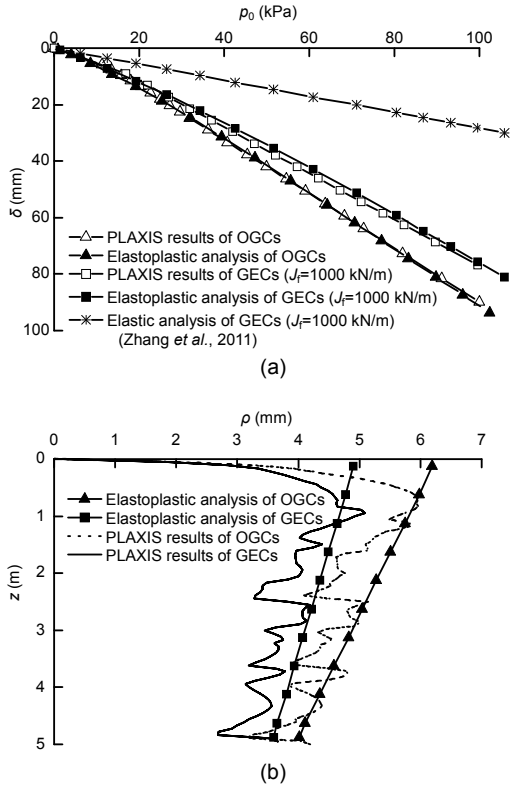

Fig. 7 Comparison between elastic analysis, elastoplastic analysis, and finite element analysis
(a) Load-settlement behavior; (b) Radial displacement vs. depth (p_0=100 kPa)

4.1 Effect of geosynthetic stiffness

The load-settlement response of the foundations with GECs with various encasement stiffnesses is shown in Fig. 8. Increasing the stiffness of the encasement can obviously reduce the settlement. This result is different from that of the elastic analyses (Zhang *et al.*, 2011). In the elastoplastic analyses, the column gradually yields in the course of loading, and increasing the encasement stiffness can defer the yielding of the column. However, in the elastic analyses, the column always remains elastic regardless of the geosynthetic stiffness and the load. The plastic settlement correction factor N decreases with increasing encasement stiffness (Fig. 9). This means that the influence of the yielding of the column becomes smaller with an encasement of higher stiffness.

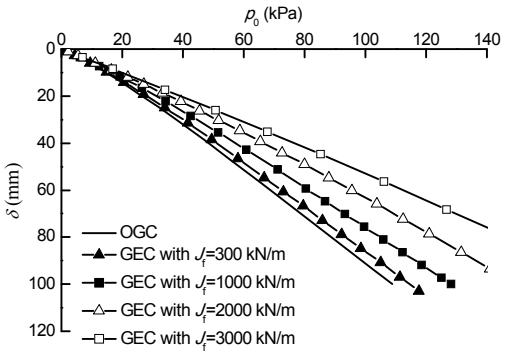

Fig. 8 Load-settlement behavior

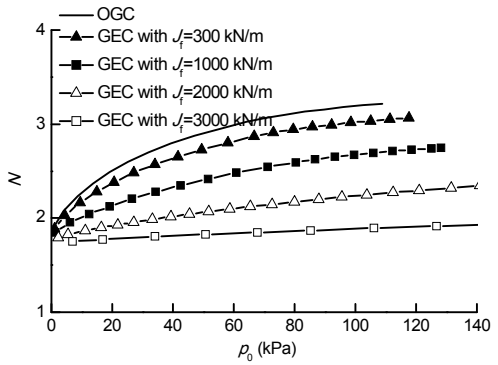

Fig. 9 Plastic settlement correction factors

The radial displacement of the column at a vertical stress of 100 kPa with various encasement stiffnesses is shown in Fig. 10. Under a load of p_0=100 kPa, the bottom of the column remains elastic when the stiffness of the encasement is over 2000 kN/m. Also, most of the column remains elastic when the stiffness of the encasement reaches 3000 kN/m. This result also highlights that increasing the encasement stiffness can delay the column's change to a plastic state.

Fig. 11 shows the mobilized load for geosynthetics with different stiffnesses at vertical settlements of 25, 50 and 100 mm. It indicates that the geosynthetic can improve the load carrying capacity of the composite foundation and that the mobilized load increases as the geosynthetic stiffness increases, especially for large settlements. We conclude that the

influence of the encasement increases with increasing settlement.

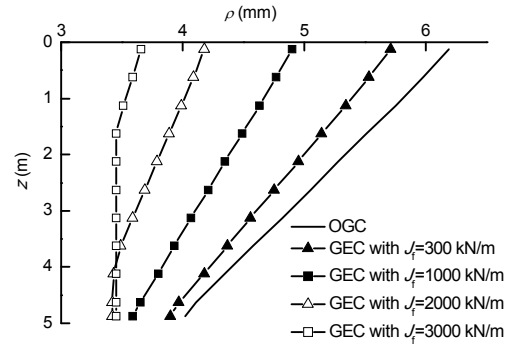

Fig. 10 Radial displacement vs. depth (p_0=100 kPa)

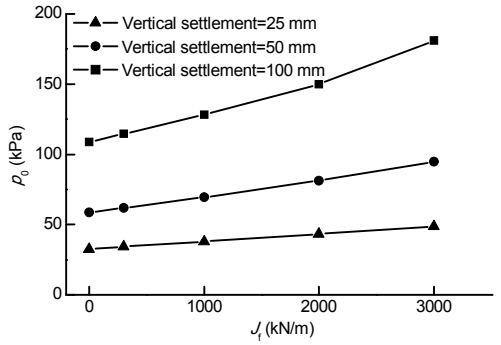

Fig. 11 Mobilized load foundation

4.2 Effect of the length of encasement

Estimating the optimum length of an encasement is of wide interest. Murugesan and Rajagopal (2006; 2007) concluded that the optimum length is $4r_c$ based on numerical analysis, and $8r_c$ based on a model test. Khabbazian *et al.* (2010) performed numerical analyses and suggested that the optimum length should be a function of the load that is applied to the column. Wu *et al.* (2009) proposed an optimum length depending on the characteristics of the in-situ soil and the stiffness and yield strength of the geosynthetic. However, the optimum length of encasement of a composite foundation has not yet been discussed.

To investigate the influence of the length of encasement on the performance of a composite foundation, the deformation of a composite foundation with an encasement length from 1 to 5 times the column diameter was calculated using our proposed method. The results of load-settlement behavior are shown in Fig. 12. Under small loading, the settlements of the composite foundation with partially encased columns are almost the same as those of fully encased columns. However, as the load increases, the influence of the length of the encasement becomes more significant, i.e., a longer encasement results in a smaller settlement.

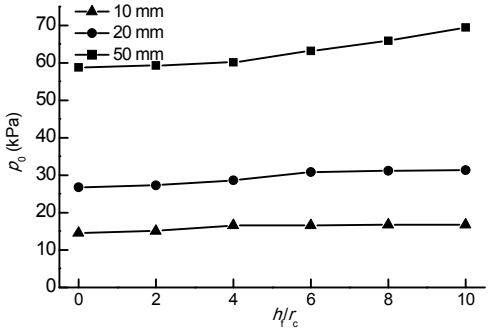

Fig. 12 Load-settlement behavior of foundation with various length of encasements

The mobilized loads for different lengths of encasement at various settlements are shown in Fig. 13, which reveals the detailed effects of the length of encasement on the performance of the GECs. For a 10 cm settlement, the effect of the encasement on the bearing capacity is no longer evident once the length reaches $4r_c$. For a 20 cm settlement, the optimal length of encasement should be taken as $6r_c$, and for a 50 cm settlement, any increase in the length of the encasement will obviously increase the bearing capacity.

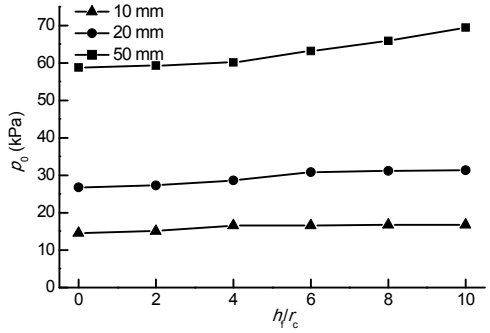

Fig. 13 Mobilized load of foundation with various lengths of encasement

Fig. 14 shows the influence of the length of encasement on the radial displacement of the column. It is clear that the existence of the geosynthetic decreases the radial displacement of the column with full encasement (h_f=10r_c). For a partially encased column, the part of the column without encasement

bulges and produces a bigger deformation than that of the OGC. Compared to the OGC, the GEC is stiffer even when it is partially encased, and it shares more vertical load. Thus, more vertical load is transferred to the part of the column without encasement, causing a larger radial displacement.

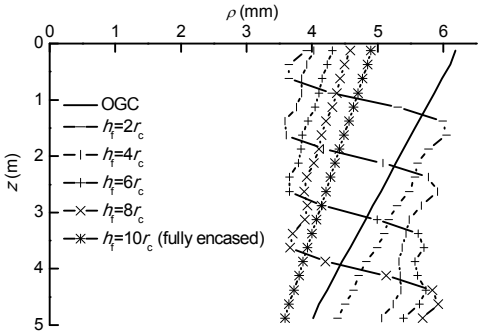

Fig. 14 Radial displacement with various lengths of encasement (p_0=100 kPa)

We conclude from the above analysis that the optimum encasing length should be determined by the permissible vertical and radial deformation, and the load acting on the foundation with GECs.

4.3 Effect of the dilation angle of granular materials

Analyses with different dilation angles of 0°, 5°, 10°, and 15° were performed to examine the influence of the dilation of granular materials on the performance of composite foundations. The results indicate that the settlement decreases with increasing dilation angle (Fig. 15), especially for a large loading. The effect of the dilation angle of granular materials on the mobilized load at various vertical settlements is shown in Fig. 16. The effect is insignificant at small displacements, but becomes evident at large displacements. The reason is that the dilatation of the column caused by shear dilation effect is more obvious at larger displacements, and therefore larger loads (Fig. 17), and the confining effect of the encasement is more obvious at larger displacements, as stated above.

4.4 Effect of the elastic modulus of the surrounding soil

To investigate the effect of GECs in different soils, the performance of a foundation with GECs was compared with that of a foundation with OGC. The ratio of mobilized load of foundation with GECs to that with OGCs (p_0^{GECs}/p_0^{OGCs}) was used to evaluate the performance of the GECs.

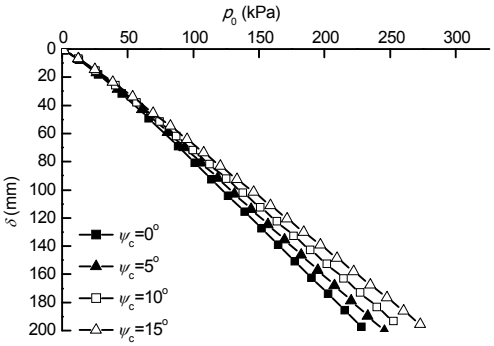

Fig. 15 Effect of the dilation angle of the column on the load-settlement behavior

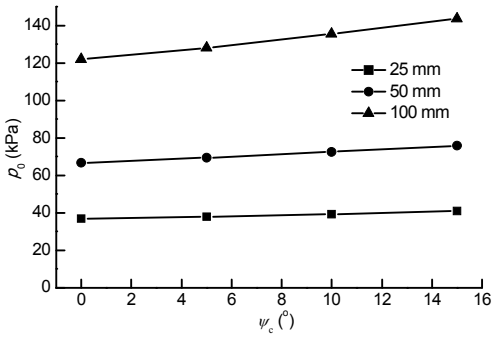

Fig. 16 Mobilized load of foundation with dilation angle of the column

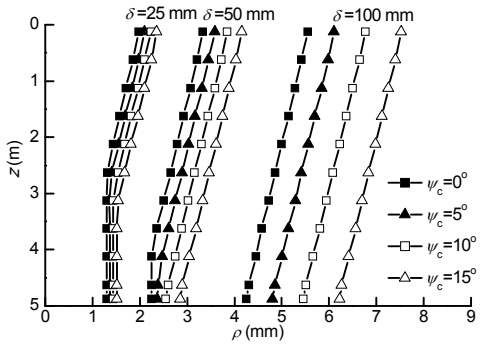

Fig. 17 Radial displacement with various dilation angles of the column

Fig. 18 shows the ratios of mobilized load for different soils at different settlements. Clearly, the mobilized load ratio is larger and the GECs work more effectively when the elastic modulus of the soil is smaller, and vice versa. We conclude that the effect

of the encasement is more significant for weak soil. Thus, GECs are more appropriate and successful for treating very weak soil.

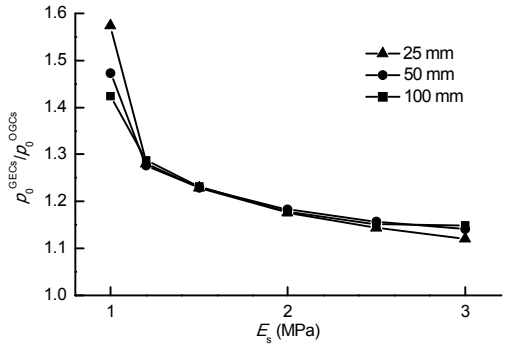

Fig. 18 Ratio of the mobilized load of foundation in soil of different elastic modulus

4 Conclusions

Based on the unit cell model and the assumption that yielding occurs in columns while no yielding occurs in the surrounding soil, an elastoplastic analytical procedure is proposed for analyzing the performance of foundations with GECs. The proposed analytical method was verified by finite element analyses using PLAXIS. Parametric analyses were carried out to study the effect of geosynthetic stiffness, the length of encasement, the dilation angle of granular materials and the elastic modulus of the soil on the performance of the composite foundations. Through the parametric analyses, the following conclusions have been reached:

1. The effect of the encasement on improving the performance of the composite foundations is significant after yielding occurs in the column. The higher is the geosynthetic stiffness, the smaller is the settlement of the composite foundations.

2. When the column is partially encased, the part of the column without encasement bulges and produces a larger deformation than that of an OGC. The radial displacement is smaller and more uniform for a fully encased column. The optimum length of encasement depends on the load acting on the foundation and the permissible vertical and radial deformation of the column.

3. The dilatancy of the granular materials has some influence on the performance of the composite foundations. Increasing the dilation angle of the column material decreases the settlement. The influence is more significant at large loads and settlements.

4. The mobilized load ratio (p_0^{GECs}/p_0^{OGCs}) is larger and the effect of the encasement is more significant when the surrounding soil has smaller elastic modulus. This implies that GECs are more suitable for very soft soil.

References

Ayadat, T., Hanna, A.M., 2005. Encapsulated stone columns as a soil improvement technique for collapsible soil. *Ground Improvement*, **9**(4):137-147. [doi:10.1680/grim.2005.9.4.137]

Balaam, N.P., Booker, J.R., 1985. Effect of stone column yield on settlement of rigid foundations in stabilized clay. *International Journal for Numerical Analytical Methods in Geomechanics*, **9**(4):331-351. [doi:10.1002/nag.1610090404]

Gniel, J., Bouazza, A., 2009. Improvement of soft soils using geogrid encased stone columns. *Geotextiles and Geomembranes*, **27**(3):167-175. [doi:10.1016/j.geotexmem.2008.11.001]

Gniel, J., Bouazza, A., 2010. Construction of geogrid encased stone columns: a new proposal based on laboratory testing. *Geotextiles and Geomembranes*, **28**(1):108-118. [doi:10.1016/j.geotexmem.2009.12.012]

Kempfert, H.G., Jaup, A., Raithel, M., 1997. Interactive Behaviour of a Flexible Reinforced Sand Column Foundation in Soft Soils. Proceedings of 14th International Conference on Soil Mechanics and Geotechnical Engineering, Hamburg, Germany, p.1757-1760.

Kempfert, H.G., Raithel, M., Jaup, A., 1999. Model Tests for Analysis of the Bearing and Deformation Behaviour of Column Foundations. 12th European Conference on Soil Mechanics and Geotechnical Engineering, Geotechnical Engineering for Transportation Infrastructure, Amsterdam, the Netherlands, p.1521-1526.

Khabbazian, M., Kaliakin, V.N., Meehan, C.L., 2009. 3D Numerical Analyses of Geosynthetic Encased Stone Columns. International Foundation Congress and Equipment Expo., Orlando, Florida, USA, p.201-208. [doi:10.1061/41023(337)26]

Khabbazian, M., Meehan, C.L., Kaliakin, V.N., 2010a. Numerical Study of Effect of Encasement on Stone Column Performance. Advances in Analysis, Modeling & Design Proceedings of the GeoFlorida Conference, West Palm Beach, Florida, USA, p.184-193. [doi:10.1061/41095(365)15]

Khabbazian, M., Kaliakin, V.N., Meehan, C.L., 2010b. Numerical study of the effect of geosynthetic encasement on the behavior of granular columns. *Geosynthetics International*, **17**(3):132-143. [doi:10.1680/gein.2010.17.3.132]

Lo, S.R., Zhang, R., Mak, J., 2010. Geosynthetic-encased stone columns in soft clay: a numerical study. *Geotextiles and Geomembranes*, **28**(3):292-302. [doi:10.1016/j.geotexmem.2009.09.015]

Lur′E, A.I., 1964. Three-Dimensional Problems of the Theory of Elasticity. John Wiley & Sons, Inc, New York-London-Sydney.

Malarvizhi, S.N., Ilamparuthi, K., 2008. Numerical Analysis of Encapsulated Stone Columns. 12th International Conference of International Association for Computer Methods and Advances in Geomechanics, Goa, India, p.3719-3726.

Murugesan, S., Rajagopal, K., 2006. Geosynthetic-encased stone columns: numerical evaluation. *Geotextiles and Geomembranes*, **24**(6):349-358. [doi:10.1016/j.geotexmem.2006.05.001]

Murugesan, S., Rajagopal, K., 2007. Model tests on geosynthetic-encased stone columns. *Geosynthetics International*, **14**(6):346-354. [doi:10.1680/gein.2007.14.6.346]

Murugesan, S., Rajagopal, K., 2010. Studies on the behavior of single and group of geosynthetic encased stone columns. *Journal of Geotechnical and Geoenvironmental Engineering*, **136**(1):129-139. [doi:10.1061/(ASCE)GT.1943-5606.0000187]

Pribe, H., 1976. Abschatzunz des setzungsverhaltens lines durch stopverdich tung verbesserten baugrundes. *Die Bautechnik*, (5):160-162 (in German).

Pulko, B., Majes, B., Logar, J., 2011. Geosynthetic-encased stone columns: analytical calculation model. *Geotextiles and Geomembranes*, **29**(1):29-39. [doi:10.1016/j.geotexmem.2010.06.005]

Raithel, M., Kempfert, H.G., 2000. Calculation Models for Dam Foundations with Geosynthetic Coated Sand Columns. International Conference on Geotechnical & Geological Engineering, Melbourne, Australia.

Rajagopal, K., Krishnaswamy, N.R., Latha, G.M., 1999. Behaviour of sand confined with single and multiple geocells. *Geotextiles and Geomembranes*, **17**(3):171-184. [doi:10.1016/S0266-1144(98)00034-X]

van Impe, W., Silence, P., 1986. Improving of the Bearing Capacity of Weak Hydraulic Fills by Means of Geotextile. Proceedings of the 3rd International Conference on Geotextiles, Vienna, Austria, p.1411-1416.

Wu, C., Hong, Y., 2009. Laboratory tests on geosynthetic-encapsulated sand columns. *Geotextiles and Geomembranes*, **27**(2):107-120. [doi:10.1016/j.geotexmem.2008.09.003]

Wu, C., Hong, Y., Lin, H., 2009. Axial stress-strain relation of encapsulated granular column. *Computers and Geotechnics*, **36**(1-2):226-240. [doi:10.1016/j.compgeo.2008.01.003]

Zhang, Y.P., Li, T., Wang, Y., 2011. Theoretical solutions for foundations improved by geosynthetic-encased stone columns. *Geosynthetics International*, **18**(1):12-20. [doi:10.1680/gein.2011.18.1.12]

Appendix

The coefficient A_{ij} was derived by Balaam and Booker (1985). However, there were some small mistakes (maybe misprints) which create difficulties for further study. Thus, this part of their work is redone here to give the correct expression of A_{ij}.

As shown in Fig. 3, the average radial displacement over the interval $z_i \le z \le z_{i+1}$ caused by radial stress R_j, when no vertical displacement occurs on the upper surface, is derived as follows.

Based on the P-N solution of the theory of elasticity, the formula of the displacements in an axisymmetric problem can be expressed as (Lur′E, 1964):

$$u_r = \frac{\lambda_s + 2G_s}{G_s} P_r^* - \frac{\lambda_s + G_s}{2G_s} \frac{\partial}{\partial r}\left(P_0 + rP_r^* + zP_z\right), \quad \text{(A1)}$$

$$u_z = \frac{\lambda_s + 2G_s}{G_s} P_z - \frac{\lambda_s + G_s}{2G_s} \frac{\partial}{\partial z}\left(P_0 + rP_r^* + zP_z\right), \quad \text{(A2)}$$

where u_r and u_z are the radial and vertical displacements, respectively. The functions P_0, P_z, and P_r^* are independent of θ. Let P_z=0, and the functions P_0 and P_r^* satisfy:

$$\left(\nabla^2 - \frac{1}{r^2}\right) P_r^* = 0, \quad \text{(A3)}$$

$$\nabla^2 P_0 = 0. \quad \text{(A4)}$$

Solving Eqs. (A3) and (A4) and substituting P_r^* and P_0 into Eqs. (A1) and (A2) obtains:

$$u_r = \sum_{i=1}^{4} c_i \Phi_i(\alpha r)\cos(\alpha z), \quad \text{(A5)}$$

$$u_z = \sum_{i=1}^{4} c_i \Psi_i(\alpha r)\sin(\alpha z), \quad \text{(A6)}$$

where $\alpha = n\pi/h$, n is integer.

The compressive stresses and deformations are taken as positive stresses and deformations.

The corresponding physical equations are:

$$\sigma_{rs} = \lambda_s \theta_s - 2G_s \frac{\partial u_r}{\partial r}, \quad \text{(A7)}$$

$$\tau_{\mathrm{rzs}}=-G_{\mathrm{s}}\left(\frac{\partial u_r}{\partial z}+\frac{\partial u_z}{\partial r}\right), \tag{A8}$$

where $\theta_{\mathrm{s}}=-\dfrac{\partial u_r}{\partial r}-\dfrac{u_r}{r}-\dfrac{\partial u_z}{\partial z}$, is the volume strain.

Substituting Eqs. (A3) and (A4) into Eqs. (A7) and (A8), we obtain:

$$r\sigma_{\mathrm{rs}}=\sum_{i=1}^{4}c_i\chi_i(\alpha r)\cos(\alpha z), \tag{A9}$$

$$r\tau_{\mathrm{rzs}}=\sum_{i=1}^{4}c_i\Omega_i(\alpha r)\sin(\alpha z), \tag{A10}$$

where c_1, c_2, c_3, and c_4 are constants and the functions Φ_i, Ψ_i, χ_i, and Ω_i are given in Table A1.

Assuming the radial stress on the inner surface is $r\sigma_{\mathrm{rs}}=\cos(\alpha z)$ ($\alpha=n\pi/h$, n is integer), when $n\neq0$, according to the displacement and stress boundary conditions, the constants c_1, c_2, c_3, and c_4 must satisfy the following equation (Balaam and Booker, 1985):

$$\begin{bmatrix}\chi_1(\alpha r_{\mathrm{c}}) & \chi_2(\alpha r_{\mathrm{c}}) & \chi_3(\alpha r_{\mathrm{c}}) & \chi_4(\alpha r_{\mathrm{c}})\\ \Omega_1(\alpha r_{\mathrm{c}}) & \Omega_2(\alpha r_{\mathrm{c}}) & \Omega_3(\alpha r_{\mathrm{c}}) & \Omega_4(\alpha r_{\mathrm{c}})\\ \Phi_1(\alpha r_{\mathrm{e}}) & \Phi_2(\alpha r_{\mathrm{e}}) & \Phi_3(\alpha r_{\mathrm{e}}) & \Phi_4(\alpha r_{\mathrm{e}})\\ \Omega_1(\alpha r_{\mathrm{e}}) & \Omega_2(\alpha r_{\mathrm{e}}) & \Omega_3(\alpha r_{\mathrm{e}}) & \Omega_4(\alpha r_{\mathrm{e}})\end{bmatrix}\begin{bmatrix}c_1\\c_2\\c_3\\c_4\end{bmatrix}=\begin{bmatrix}1\\0\\0\\0\end{bmatrix}. \tag{A11}$$

So the radial deflection of the inner boundary $u_r(r_{\mathrm{c}})$ is given by

$$u_{\mathrm{r}}(r_{\mathrm{c}})=k(\alpha)\cos(\alpha z), \tag{A12}$$

where $k(\alpha)=\sum_{i=1}^{4}c_i\Phi_i(\alpha r_{\mathrm{c}})$.

The specific case $\alpha=0$ can be obtained from the elastic solution (Zhang *et al.*, 2011):

$$u_0(r)=-\frac{\dfrac{r}{r_{\mathrm{c}}}\left(1-\dfrac{r_{\mathrm{e}}^2}{r_{\mathrm{c}}^2}\right)}{2\left[\lambda_{\mathrm{s}}+G_{\mathrm{s}}\left(1+r_{\mathrm{e}}^2/r_{\mathrm{c}}^2\right)\right]}, \tag{A13}$$

then

$$k(0)=-\frac{\left(1-r_{\mathrm{e}}^2/r_{\mathrm{c}}^2\right)}{2\left[\lambda_{\mathrm{s}}+G_{\mathrm{s}}\left(1+r_{\mathrm{e}}^2/r_{\mathrm{c}}^2\right)\right]}. \tag{A14}$$

Finally, the situation in which the inner surface is subjected to a radial stress distribution over the interval $z_i\leq z\leq z_{i+1}$ caused by R_j can be expressed as

$$\sigma_{\mathrm{rs}}(r_{\mathrm{c}})=\begin{cases}\dfrac{R_j}{2\pi r_{\mathrm{c}}\Delta z_j}, & z\in\left[z_j,z_{j+1}\right],\\ 0, & z\in\left[0,z_j\right)\cup\left(z_{j+1},h\right].\end{cases} \tag{A15}$$

Then, using the theory of Fourier series, the radial stress on the inner boundary is subdivided into several cosine functions:

$$r_{\mathrm{c}}\sigma_{\mathrm{rs}}(r_{\mathrm{c}})=\frac{R_j}{h\pi}\left[\frac{1}{2}+\sum_{n=1}^{\infty}f_{nj}\cos(\alpha_n z)\right], \tag{A16}$$

Table A1 Definitions of functions Φ_i, Ψ_i, χ_i, and Ω_i*

$\Phi_1(\alpha r)=\dfrac{\lambda_{\mathrm{s}}+2G_{\mathrm{s}}}{G_{\mathrm{s}}}I_1(\alpha r)-\dfrac{\lambda_{\mathrm{s}}+G_{\mathrm{s}}}{2G_{\mathrm{s}}}\alpha rI_0(\alpha r)$,
$\Phi_2(\alpha r)=\dfrac{\lambda_{\mathrm{s}}+2G_{\mathrm{s}}}{G_{\mathrm{s}}}K_1(\alpha r)+\dfrac{\lambda_{\mathrm{s}}+G_{\mathrm{s}}}{2G_{\mathrm{s}}}\alpha rK_0(\alpha r)$,
$\Phi_3(\alpha r)=-K_1(\alpha r)$,
$\Phi_4(\alpha r)=K_0(\alpha r)$.
$\Psi_1(\alpha r)=\dfrac{\lambda_{\mathrm{s}}+G_{\mathrm{s}}}{2G_{\mathrm{s}}}\alpha rI_1(\alpha r)$,
$\Psi_2(\alpha r)=\dfrac{\lambda_{\mathrm{s}}+G_{\mathrm{s}}}{2G_{\mathrm{s}}}\alpha rK_1(\alpha r)$,
$\Psi_3(\alpha r)=I_0(\alpha r)$,
$\Psi_4(\alpha r)=K_0(\alpha r)$.
$\chi_1(\alpha r)=(4G_{\mathrm{s}}+2\lambda_{\mathrm{s}})I_1(\alpha r)-(3G_{\mathrm{s}}+2\lambda_{\mathrm{s}})\alpha rI_0(\alpha r)+(G_{\mathrm{s}}+\lambda_{\mathrm{s}})\alpha^2r^2I_1(\alpha r)$,
$\chi_2(\alpha r)=(4G_{\mathrm{s}}+2\lambda_{\mathrm{s}})K_1(\alpha r)+(3G_{\mathrm{s}}+2\lambda_{\mathrm{s}})\alpha rK_0(\alpha r)+(G_{\mathrm{s}}+\lambda_{\mathrm{s}})\alpha^2r^2K_1(\alpha r)$,
$\chi_3(\alpha r)=-2G_{\mathrm{s}}(I_1(\alpha r)-\alpha rI_0(\alpha r))$,
$\chi_4(\alpha r)=2G_{\mathrm{s}}(K_1(\alpha r)+\alpha rK_0(\alpha r))$.
$\Omega_1(\alpha r)=-(\lambda_{\mathrm{s}}+G_{\mathrm{s}})\alpha^2r^2I_0(\alpha r)+(\lambda_{\mathrm{s}}+2G_{\mathrm{s}})\alpha rI_1(\alpha r)$,
$\Omega_2(\alpha r)=(\lambda_{\mathrm{s}}+G_{\mathrm{s}})\alpha^2r^2K_0(\alpha r)+(\lambda_{\mathrm{s}}+2G_{\mathrm{s}})\alpha rK_1(\alpha r)$,
$\Omega_3(\alpha r)=-2G_{\mathrm{s}}\alpha rI_1(\alpha r)$,
$\Omega_4(\alpha r)=2G_{\mathrm{s}}\alpha rK_1(\alpha r)$.

* I_0 and I_1 are the first kind zero- and one-order modified Bessel functions, respectively; K_0 and K_1 are the second kind zero- and one-order modified Bessel functions, respectively

where $\alpha_n=n\pi/h$, $f_{nj}=(\sin(\alpha_n z_{j+1})-\sin(\alpha_n z_j))/(\alpha_n \Delta z_j)$.

The radial deflection on the inner surface of the problem can be obtained by superposing the elementary solution:

$$u_r(r_c)=\frac{R_j}{h\pi}\left[\frac{k(0)}{2}+\sum_{n=1}^{\infty} f_{nj}k(\alpha_n)\cos(\alpha_n z)\right]. \quad \text{(A17)}$$

So the average deflection $(\rho_1)_{ij}$ over the interval $z_i \le z \le z_{i+1}$ caused by R_j is given by

$$(\rho_1)_{ij}=\frac{R_j}{h\pi}\left[\frac{k(0)}{2}+\sum_{n=1}^{\infty} f_{nj}k(\alpha_n)f_{ni}\right]. \quad \text{(A18)}$$

Referring to Eq. (1), we obtain:

$$A_{ij}=A_{ji}=\frac{1}{h\pi}\left[\frac{k(0)}{2}+\sum_{n=1}^{\infty} f_{nj}k(\alpha_n)f_{ni}\right]. \quad \text{(A19)}$$